2024 IEEE/RSJ International Conference on Intelligent Robots and Systems (IROS)
October 14-18, 2024. Abu Dhabi, UAE

A Closed-loop Control for Lower Limb Exoskeleton Considering Overall Deformations: A Simple and Direct Application Method

Feng Li[1,2], Ming Yang[3], Ziqiang Chen[1,2], Mengbo Luan[1,2], Dingkui Tian[1] and Xinyu Wu[1]
Senior Member, IEEE

***Abstract*— In this paper, considering overall deformations of the exoskeleton, we couple deformations relationship network (DRN) with fractional order viscoelastic (FOV) controller, proposing a novel DRN-FOV closed-loop control method, endowing exoskeleton with stable dynamic walking ability. Simply by utilizing only the data from the 6-axis force/torque sensors, the DRN can directly capture the mapping relationship between the foot reaction force/torque of the exoskeleton and its overall deformations. We introduce the FOV to eliminate disturbances and stabilize during walking tasks. The closed-loop control method directly compensates for the overall deformations of the exoskeleton and enables the wearer to walk stably wearing the exoskeleton. To assess the effectiveness of the proposed control method, walking tasks were effectively carried out on subjects with varying body parameters using the developed exoskeleton. The experimental results show that the DRN-FOV closed-loop control method accurately estimates and compensates for deformations, resulting in an improved dynamic walking ability of the exoskeleton with wearers.**

I. INTRODUCTION

Lower limb exoskeletons (LLEs) are designed as intelligent devices to enhance human mobility. They enhance the performance of unimpaired individuals while also restoring movement in individuals with gait impairments [1], [2]. The LEEs should enable wearers to achieve dynamic walking without the need for external assistance, resulting in a more optimal and natural gait pattern, similar to the gait of bipedal robots [3], [4]. Unlike bipedal robot systems [5], achieving dynamic hands-free walking for LLEs systems is a challenging problem [6]. This is because all LLEs control laws provide a certain degree of freedom to the wearers, meaning that the exoskeleton is not a completely rigid mechanical structure [7], [8]. These challenges include accurate estimation of the deformations of the LLEs during walking [9], [10], as well as the generalizability of stablize the LLEs to users with varying body weights [11].

This work was supported in part by National Natural Science Foundation of China (Grants No. 62125307 and 62373346), in part by Shenzhen Science and Technology Program (Grant No. JCYJ20220818101416035), in part by Shenzhen Medical Research Fund Grant B2302002, in part by Shenzhen Science and Technology Program (Grant No. RCBS20231211090523046). (Corresponding author: Xinyu Wu.)

[1] Feng Li, Ziqiang Chen, Mengbo Luan, Dingkui Tian and Xinyu Wu are with the Shenzhen Institute of Advanced Technology, Chinese Academy of Sciences, Shenzhen 518005, China, and with the Guangdong Provincial Key Lab of Robotics and Intelligent System, Shenzhen Institute of Advanced Technology, Chinese Academy of Sciences, Shenzhen 518005, China. {feng.li, zq.chen, mb.luan, dk.tian1, xy.wu} @siat.ac.cn.

[2] Feng Li, Ziqiang Chen and Mengbo Luan are also with the University of Chinese Academy of Sciences, Beijing 100190, China.

[3] Ming Yang is with the University of Science and Technology of China, Hefei 230026, China. yangming_@mail.ustc.edu.cn.

Fig. 1. The developed lower limb exoskeleton, close-up view (left) and the user wearing the exoskeleton (right). The yellow link represents the ideal rigid body state, while the blue link represents the actual exoskeleton state. Videos can be accessed online [33].

More specifically, heavier the LLEs not only need to support their own weight but also the weight of the wearer [12], [13]. For many LLEs, the hypothesis of full rigidity does not exist. The mechanical structure of these robots needs to provide users with enough space for movement and support the weight of the wearers [14], [15]. These mechanical constraints often lead to deformations of the LLEs. This is the situation encountered by the LLEs we developed, see Fig. 1. Hence, accurately estimating and compensating for the deformations of LLEs using intelligent controllers to enable hands-free stable walking for the wearers is a key challenge in the wearable exoskeleton field. Moreover, generalizing this approach across different human body parameters effectively is essential.

Recent research has concentrated on creating a hands-free stable walking controller for the LLEs, as well as accurately estimating the deformations state of the LLEs. Vigne et al. proposed an estimation method using several IMUs and motion capture to reconstruct the state of multiple deformations during the LLEs walking [10]. Further, Vigne et al. extends the estimation method to build an estimator for multiple deformations considering acceleration [14]. Brunet et al. proposed an online gait replanning method for exoskeleton, which relies on simple robot dynamics models to achieve stable walking of robots in the presence of external

disturbances [16]. Although their proposed approach may not be universally applicable, it has the potential to be expanded to include deformations of the LLEs. Stable walking patterns were developed using a combination of hybrid zero dynamic and partial hybrid zero dynamic frameworks to enable dynamic exoskeleton walking without the need for crutches [17], [18]. Xavier et al. designed the state estimator calculator to provide trajectory and deformations estimation of the exoskeleton through data from multiple IMU sensors [19]. However, such IMU-based deformations estimation methods have inherent inaccuracies and biases, complex calculations, and requires the parameters to be tuned as needed [20], [21]. Thus, the primary objective of this paper is to create a simple closed-loop integrated controller that employs a limited number of sensors to directly assess the overall deformations of the exoskeleton.

This paper presents a simple and direct closed-loop control method for accurate estimation of overall deformations of the LLEs and generalization across subjects of different body parameters. We have developed an end-to-end direct deformations relation network that utilizes only one type of sensor - the 6-axis force/torque (F/T) sensor to predict the overall deformations of the LLEs. This approach draws inspiration from the self-attention mechanism [22], [23] and the sparsity characteristic of CNN [24], [25]. The proposed deformations relation network enhances its capability to comprehend contextual information within input sequences, making it particularly suitable for analyzing gait periodic data. By incorporating a self-attention mechanism, the network can effectively highlight and analyze pertinent information across various gait cycles. Furthermore, our implementation also includes a fractional-order viscoelastic controller, which can reduce the vibration of the exoskeleton during walking [26]. The attenuation of vibration is due to the memory and hereditary advantages of fractional calculus [27], [28]. In the field of control, the advantage of small energy consumption of fractional order has been demonstrated [29]. The fractional order viscoelastic controller introduces compliance to the exoskeleton, reducing vibration during exoskeleton movement. The main contribution of the paper can be summarized as follows:

- A simple and direct closed-loop control method, known as DRN-FOV, is proposed to address the deformations of the LLEs and stabilize the LLEs for walking. This method involves utilizing a 6-axis F/T sensors to accurately capture and compensate for the overall deformations of the LLEs in each control cycle.
- The proposed control method has been applied and validated in walking experiments with five wearers of different body parameters.

II. Problem Definition

This section defines the inputs and outputs of the deformation problem of the exoskeleton.

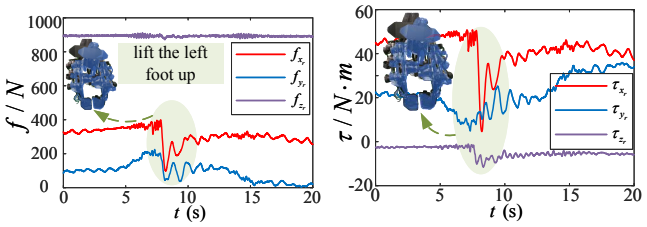

(a) Force trend (b) Torque trend

Fig. 2. The process of analyzing the deformations of the exoskeleton. The trend of force and torque changes in the right foot (supporting foot) during the left foot lifting phase.

A. deformations analysis

In the deformations analysis experiment, the LLEs system was evaluated without our proposed method. Fig. 1 (right) shows the pose of the LLEs when lifting the left foot. As can be seen from the local amplification of the figure, both the supporting and swinging feet are not parallel to the ground, resulting in the exoskeleton tilting. The actual center of mass (CoM) of the exoskeleton (blue ball, $\mathbf{T}_{CoM}^{real}$) is situated at a lower height compared to the reference CoM (yellow ball, $\mathbf{T}_{CoM}^{ref}$). The blue link and the yellow link of the LLEs are not completely consistent.

In addition, we quantitatively analyze the deformations of exoskeleton. The variations in the force and torque of the support foot (right foot) are collected. As shown in Fig. 2, during the moment of lifting the left foot of the exoskeleton, there is a significant abrupt change in the forces and torques of the support foot in the X and Y directions. The X axis represents the sagittal plane of the LLEs, and the Y axis represents the frontal plane of the LLEs. For instance, f_{x_r} jump from 400 N to 100 N, f_{y_r} jump from 200 N to 50 N, and the τ_{x_r} jump from 49 Nm to 5 Nm, τ_{y_r} jump from 5 Nm to 30 Nm, where f_{x_r} represents the force of the right foot in the X axis direction, τ_{x_r} represents the torque of the right foot in the X axis direction, and the other symbols follow suit.

In an ideal situation, the support foot of the exoskeleton would only have changes in force and torque in the Z direction, while there would be no significant changes in the X and Y directions. However, the presence of deformation of the exoskeleton causes the support foot of the abrupt changes in forces and torques in the X and Y directions. The LLEs tilts to the side of the swinging foot (blue robot state) and loses balance to walk normally.

B. Direct mapping of deformations

As shown in Fig. 2, the overall deformations of the exoskeleton has a significant impact on the changes in force and torque $\mathrm{F} = \begin{bmatrix} \mathrm{F}_l & \mathrm{F}_r \end{bmatrix}^{\mathrm{T}} \in \mathbb{R}^{12}$, where $\mathrm{F}_l = \begin{bmatrix} f_{x_l} & f_{y_l} & f_{z_l} & \tau_{x_l} & \tau_{y_l} & \tau_{z_l} \end{bmatrix}^{\mathrm{T}} \in \mathbb{R}^6$ denotes the matrix of forces and torques of the left foot and $\mathrm{F}_r = \begin{bmatrix} f_{x_r} & f_{y_r} & f_{z_r} & \tau_{x_r} & \tau_{y_r} & \tau_{z_r} \end{bmatrix}^{\mathrm{T}} \in \mathbb{R}^6$ denotes the matrix of force and torque of the right foot. The extent of changes in force and torque also reflects the degree of

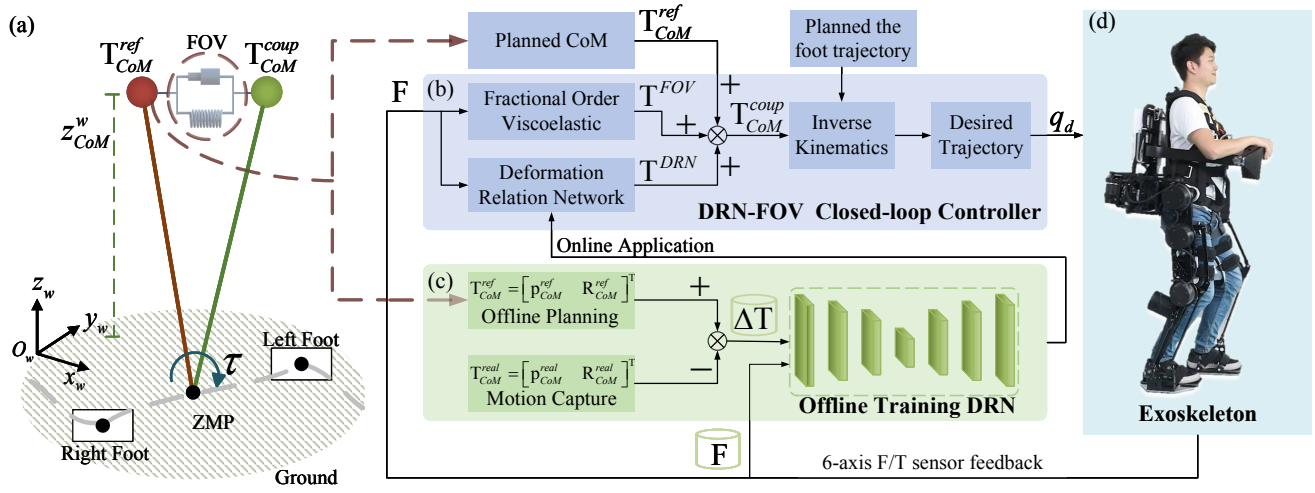

Fig. 3. The proposed comprehensive framework for closed-loop control consists of: (a) Exoskeleton dynamics model based on a linear inverted pendulum. (b) The proposed DRN-FOV closed-loop controller. (c) The offline training of the DRN. (d) The exoskeleton system

deformations. In other words, there is a nonlinear mapping relationship between F and overall deformations. The changes in the foot force and torque of the LLEs directly reflect its degree of overall deformations.

To represent deformations using mathematical methods, we use the offset of the CoM (ΔT) to indicate the overall deformations of the exoskeleton. The $\Delta \mathrm{T} = \left[\begin{array}{cc} \Delta \mathrm{p} & \Delta \mathrm{R} \end{array} \right]^{\mathrm{T}} \in \mathbb{R}^6$ includes three-dimensional (3D) position and 3D rotation, i.e., $\Delta \mathrm{p} = \left[\begin{array}{ccc} \Delta x_{com} & \Delta y_{com} & \Delta z_{com} \end{array} \right]^{\mathrm{T}}$ and $\Delta \mathrm{R} = \left[\begin{array}{ccc} \Delta \alpha_{com} & \Delta \beta_{com} & \Delta \gamma_{com} \end{array} \right]^{\mathrm{T}}$. The change of F directly reflects the change of ΔT. Solving for ΔT using F is a nonlinear problem and can be expressed as

$$\Delta \mathrm{T} = f^{\Delta}(\mathrm{F}), \tag{1}$$

where $f^{\Delta}(\cdot)$ represents a nonlinear mapping function. The position and rotation of ΔT in 3D space can represent the degree of overall deformations of the exoskeleton in any direction and position in 3D space. Therefore, it is reasonable to simply transform the overall deformations of LLEs into the offset of CoM.

III. Control Method

In this section, we present our main contribution— a direct control method to address deformations of the LLEs and enable compliant walking of the LLEs.

The core of this letter is to establish a simple and direct closed-loop control method, namely DRN-FOV. As shown in Fig. 3 (a), a centroid dynamic model of exoskeleton based on a linear inverted pendulum (LIP) is established to generate reference trajectories for the CoM and foot placements. The collected deformations data are utilized for offline training of the DRN to create a mapping network directly correlating force to deformations compensation, as shown in Fig. 3 (c). Next, the design process of fractional order viscoelastic (FOV) and deformations relation network (DRN) are described in detail.

A. Design of the fractional order viscoelastic controller

Aiming at the control purpose of adaptive and stable walking in LLEs system, the purpose of this section can be expressed as:

$$(X_{zmp}, Y_{zmp}) \in \mathrm{S}, \tag{2}$$

where the S denotes the support area of both feet. The feedback controller is designed to satisfy that the actual zero moment point (ZMP) position is always within the support surface of both feets S, so that the LLEs system keeps stable in every control cycle.

1) Generation of reference trajectories: As shown in Fig. 3 (a), we simplified the LLEs model based on centroid dynamics, which is a low-dimensional control model widely used in the field of robotics, and follow [30]. Centroid dynamics can directly describe the motion of LLEs by specifying the CoM and foot placements. We assume that LLEs walk on flat ground, meaning that the CoM height remains constant. The ZMP can be expressed as follows:

$$\begin{cases} x_p^w = x^w - \frac{z_{CoM}^w}{g} \ddot{x}^w, \\ y_p^w = y^w - \frac{z_{CoM}^w}{g} \ddot{y}^w. \end{cases} \tag{3}$$

where $\left[\begin{array}{ccc} x_p^w & y_p^w & z_p^w \end{array} \right]^{\mathrm{T}}$ and $\left[\begin{array}{ccc} x^w & y^w & z^w \end{array} \right]^{\mathrm{T}}$ denote the ZMP position and the CoM position in Σ_W, respectively. g is acceleration due to gravity. z_{CoM}^w is the height of the CoM in Σ_W.

The movements of the LLEs system in the sagittal and frontal planes are independent and have the same form of movement. In the sagittal plane, the state equation can be discretized at a sampling step T_s as

$$\begin{aligned} x(k+1) &= \Phi x(k) + \mathrm{H}(u_{\mathrm{c}}(k) + \eta_{\mathrm{d}}(k)) \\ y(k) &= \mathrm{G}x(k) \end{aligned} \tag{4}$$

where $\Phi = \begin{bmatrix} 1 & T_s & {T_s}^2/2 \\ 0 & 1 & T_s \\ 0 & 0 & 1 \end{bmatrix}$, $\mathrm{H} = \begin{bmatrix} {T_s}^3/6 \\ {T_s}^2/2 \\ T_s \end{bmatrix}$, and $\mathrm{G} = \begin{bmatrix} 1 & 0 & -1/\omega^2 \end{bmatrix}$. $\omega = \sqrt{g/z_{CoM}^w}$ denotes the inherent frequency of the state equation. $x(k) = \begin{bmatrix} x_m^w(kT_s) & \dot{x}_m^w(kT_s) & \ddot{x}_m^w(kT_s) \end{bmatrix}^{\mathrm{T}}$ and $y(k)$ represents the ZMP at time of k. The $\eta_d(k)$ denotes the overall deformations.

Through Eq. 4, the reference trajectory of the exoskeleton CoM and the foot placements can be obtained, allowing for the calculation of the ZMP. In offline trajectory generation, by initially setting the ZMP and foot placement trajectories, the response trajectory of the exoskeleton CoM can be determined through the following optimization problem:

$$J = \sum_{i=k}^{\infty} \left\{ Q_1 \Delta y(i)^2 + \Delta x(i)^T Q_2 \Delta x(i) + Q_3 \Delta u_c(i)^2 \right\}, \tag{5}$$

where $\Delta y(i) = y(i+1) - y_d(i)$, $\Delta x(i) = x(i) - x(i-1)$, and $\Delta u_c(i) = u_c(i) - u_c(i-1)$ are the incremental ZMP, incremental state vector and incremental input, respectively. Q_1 and Q_3 are positive definite matrices and Q_2 is a symmetric non-negative definite matrix.

To minimize J, N steps are performed in each control cycle to obtain control inputs, and the solution of Eq. 5 can be written as follows:

$$u_c(k) = -K_1 \sum_{i=0}^{k} \Delta y - K_2 x(k) - \sum_{j=0}^{N} K_3(j)\, y_d(k+j), \tag{6}$$

where K_1, K_2 and K_3 are the gain matrices obtained by solving Eq. 5.

Therefore, the reference CoM trajectories of the LLEs in the sagittal plane can be obtained based on the centroid dynamics. Similarly, the reference CoM trajectories in the frontal plane can be computed.

2) FOV controller: As shown in Fig. 3 (a), we place a FOV model between the coupled CoM and the reference CoM, which connects the real CoM and the reference CoM, enabling the system to exhibit compliant viscoelastic behavior [31]. The active torque τ provides viscoelasticity to maintain the stability of the LLEs. The torque error between the actual CoM and the reference CoM is expressed as:

$$\Delta\tau = \mathrm{F}_v z_{CoM}^w, \tag{7}$$

where $\Delta\tau = \tau^{real} - \tau^{ref}$, τ^{real} and τ^{ref} denote the real and reference torque, respectively. The F_v denotes the virtual force calculated by the FOV model, and can be expressed as:

$$\mathrm{F}_v = \mathrm{E}\Delta\mathrm{T}_{CoM} + \eta D^{\alpha}\left[\Delta\mathrm{T}_{CoM}\right], \tag{8}$$

where $\Delta\mathrm{T}_{CoM}$ represent the difference between the real CoM and the reference CoM. E and η is the spring and damping parameter of FOV model, respectively. $D^{\alpha}[\cdot]$ is a fractional order function. The implementations fractional order differential based on the $Grünwald–Letnikov$ definition is expressed as:

$$D^{\alpha}\left[x(i)\right] = \lim_{T\to 0}\left[\frac{1}{T^{\alpha}} \sum_{k=0}^{r} \frac{(-1)^k \Gamma(\alpha+1)\, x(i-kT)}{\Gamma(k+1)\,\Gamma(\alpha-k+1)}\right], \tag{9}$$

where $x(i) = \Delta\mathrm{T}_{CoM}(i)$, $\Gamma(\cdot)$ is the gamma function, T is the sampling period and r is the truncation order. Preliminary tests of fractional order differential presented similar results for $r \geq 4$. Thus, combining Eq. 7-Eq. 9 gives the FOV expression in discrete form:

$$\Delta\mathrm{T}_{CoM}(i) = \frac{T^{\alpha}\Delta\tau + z_{CoM}^w \eta\lambda}{(\eta + T^{\alpha}\mathrm{E})\, z_{CoM}^w}, \tag{10}$$

where λ is defined as follows:

$$\begin{aligned} \lambda =& \alpha\Delta\mathrm{T}_{CoM}(i-1) + \frac{1}{2}\alpha(1-\alpha)\Delta\mathrm{T}_{CoM}(i-2) + \\ & \frac{1}{6}\alpha(1-\alpha)(2-\alpha)\Delta\mathrm{T}_{CoM}(i-3) + \frac{1}{24}\alpha(1-\alpha) \\ & (2-\alpha)(3-\alpha)\Delta\mathrm{T}_{CoM}(i-4). \end{aligned} \tag{11}$$

The transformation of $\Delta\mathrm{T}_{CoM}(i)$ from the base frame to the global frame is derived:

$$\mathrm{T}^{FOV}(i) =_b^w \mathrm{R}\Delta\mathrm{T}_{CoM}(i). \tag{12}$$

Eq. 10 and Eq. 11 are FOV controller that generate a new $\Delta\mathrm{T}_{CoM}(i)$ using the data from the 6-axis F/T sensors and the previous four cycles of $\Delta\mathrm{T}_{CoM}$. The level of compliance for the controller can be adjusted through the parameters α, E and η of the FOV model. However, the overall deformations η_d in the state equation (Eq. 4) still needs to be estimated.

B. Design of the deformations relation network

To accurately estimate the overall deformation $\eta_d(k)$ of the LEEs, we designed the framework of the deformation relation network (DRN) as shown in Fig. 4. The model take the raw 6-axis F/T data as inputs and provided estimation of exoskeleton deformations variables as outputs. The architecture of the DRN combines the encoder-decoder, multi-head self-attention mechanism, and CNN to establish dependencies, filter elements, and sparse features within the DRN. The receptive field of the CNN is relatively small and captures subtle changes, thus preserving the dynamic characteristics of the feature matrix before and after the input and output. This creates a solid connection to the deformations of the LLEs.

The core of DRN is the multi-head self-attention mechanism, a module that considers any part of the input sequence from which valid feature information can be extracted. During the data processing phase, three distinct sets of vectors are generated, namely the query, the key, and the value vectors, which are denoted as $\mathrm{Q} \in \mathrm{R}^{\mathrm{L_Q}\times\mathrm{d}}$, $\mathrm{K} \in \mathrm{R}^{\mathrm{L_K}\times\mathrm{d}}$, and $\mathrm{V} \in \mathbb{R}^{\mathrm{L_V}\times\mathrm{d}}$, respectively. L_Q, L_K and L_V denote the

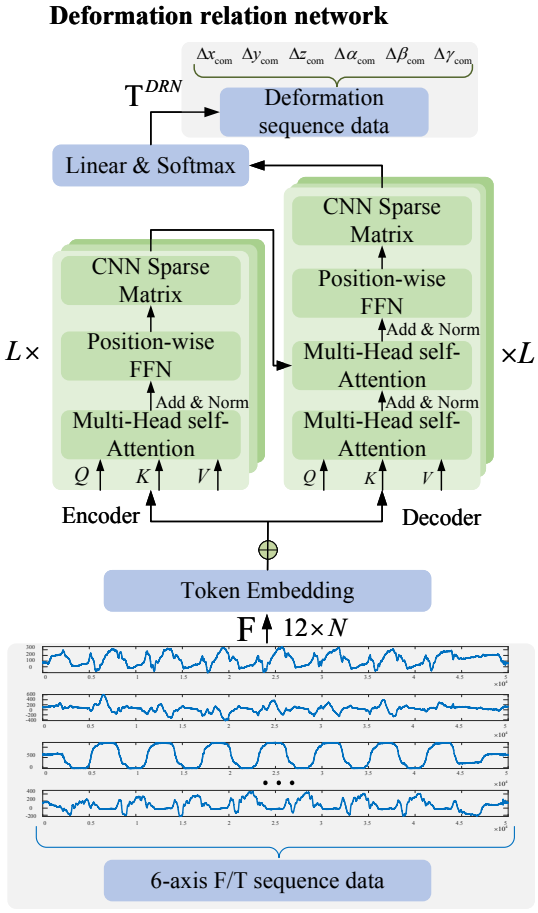

Fig. 4. Deformations relation network: a direct method for exoskeleton deformations estimation, incorporating an encoder-decoder, a multi-head self-attention mechanism, and CNN sparse matrices.

lengths of the queries, keys and values. d represents the dimensions of all vectors. Multi-head attention is written as:

$$\begin{aligned} &\mathrm{MultiHeadA(Q,K,V)} = \mathrm{Concat}(head_1, \ldots, head_H)\mathrm{W^O}, \\ &\mathrm{head}_i = \mathrm{A}(\mathrm{QW}_i^Q, \mathrm{KW}_i^K, \mathrm{VW}_i^V). \end{aligned} \tag{13}$$

where $\mathrm{A(Q,K,V)} = \mathrm{Softmax}\left[\frac{\mathrm{QK^T}}{\sqrt{d}}\right]\mathrm{V}$ is called the attention matrix. Literature provides detailed information on the various approaches for utilizing the multi-head attention mechanism [22].

In the designed of DRN, the encoder consists of multi-head attention mechanisms and position-wise feedforward network, with CNN for sparse features. In the decoder, Q matrix is generated by multi-head self-attention, and a self-attention is performed on this matrix with the K and V matrices outputted by the encoder, with CNN for sparse features. Finally, a fully connected layer (Linear & Softmax) is used to map the outputs to T^{DRN}.

As shown in Fig. 3 (c), the training data for the DRN model was collected using the NOKOV motion capture system, and our previous work details the data acquisition process [32]. The model is built on the PyTorch platform, and a GeForce RTX 3070 Ti GPU is used to train the model.

TABLE I
THE RECRUITED SUBJECTS INFORMATION

Subject	Gender	Height(cm)	Weight(kg)
S1	Male	168	59
S2	Male	172	66
S3	Male	168	60
S4	Male	175	70
S5	Male	173	66

The encoder and decoder of DRN consist of 4 blocks, with each multi-head attention layer configured with 8 heads. The dropout rate was set to 0.3. The solver used the Adam optimizer.

C. DRN-FOV control framework

As shown in Fig. 3 (b), the FOV and DRN method generate T^{FOV} and T^{DRN} online, respectively. By combining the reference CoM T_{CoM}^{ref}, the T_{CoM}^{coup} can be expressed as:

$$\mathrm{T}_{CoM}^{coup} = \mathrm{T}_{CoM}^{ref} + \mathrm{T}^{FOV} + \mathrm{T}^{DRN}, \tag{14}$$

where T_{CoM}^{coup} denotes the compensated coupled CoM. Combined with the offline planning of the foot placements, we employ an analytical approach to solve the inverse kinematics in real-time, resulting in unique joint motion trajectories for the LLEs [33].

IV. EXPERIMENT RESULTS

In this section, we describe the developed LLEs hardware, the experimental methods and the results analysis.

A. Exoskeleton prototype

As shown in Fig. 3 (d), the exoskeleton has twelve powered DOFs to generate all the joint movements of the lower limbs [33]. Three motors control the spherical motion of each hip joint, while a single motor for each knee in the sagittal plane, and two joints for each ankle rotation in the sagittal and frontal planes. Two 6 axis F/T sensors are attached to the bottom of each foot for detecting ground reactive force between foot and ground. The exoskeleton developed utilized next unit of computing (NUC) to build a real-time operating system for controller development. The control frequency was set to 250 Hz.

B. Experimental scheme

We designed walking experiments on flat ground with wearers wearing exoskeletons. In particular, five subjects with different physical were recruited to wear the LLEs for experiments. As can be seen from Table I, the body parameters of the five subjects are different, which provides ample experimental conditions for validating our method. There was an investigator who monitored the progress of the study and ensured the safety of the subjects during all experiments. The subjects did not use any aids during the whole experiment. These experiments were conducted in the laboratory of the Shenzhen Institutes of Advanced Technology, Chinese Academy of Sciences. The experiments were approved with IRB No. SIAT-IRB-200715-H0512.

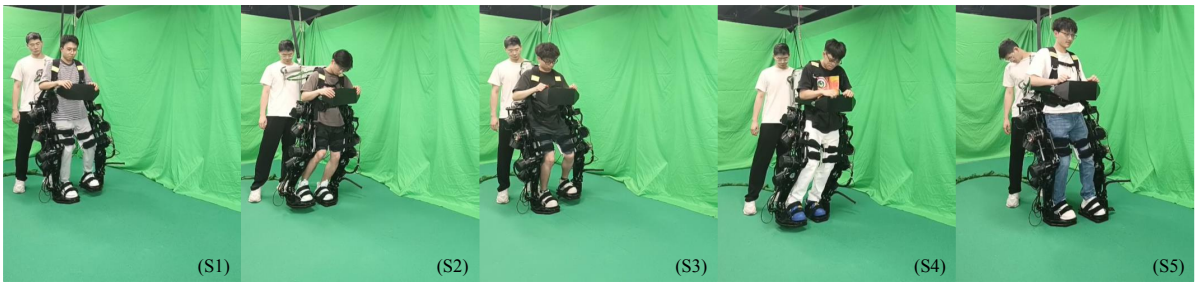

Fig. 5. A snapshot of the walking experiment for five subjects. Videos are available online [34].

TABLE II

STATISTICAL RESULTS OF THE MEAN OF ZMP ERRORS AND THE MEAN OF CONTROL VALUES FOR ALL SUBJECTS DURING THE WALKS

Subject	DRN (mm)			DRN (°)			FOV (mm)		ZMP error (m)	
	x^{DRN}	y^{DRN}	z^{DRN}	α^{DRN}	β^{DRN}	γ^{DRN}	x^{FOV}	y^{FOV}	X	Y
S1	14.08	16.16	36.84	3.99	4.98	2.77	0.6	1.8	0.0118	0.0113
S2	14.88	18.85	38.63	3.29	4.93	2.61	1.9	2.4	0.0345	0.0143
S3	14.34	15.96	36.88	4.03	4.99	2.73	0.5	2.7	0.0117	0.0161
S4	14.62	16.64	39.29	2.88	4.96	2.60	1.7	1.9	0.0324	0.0139
S5	13.99	18.51	36.59	3.99	4.96	2.75	0.7	1.8	0.0161	0.0137
Mean	14.38	17.22	37.64	3.63	4.96	2.69	1.08	2.12	0.0213	0.0138
± SE	0.33	1.21	1.09	0.47	0.02	0.07	0.59	0.36	0.01	0.001

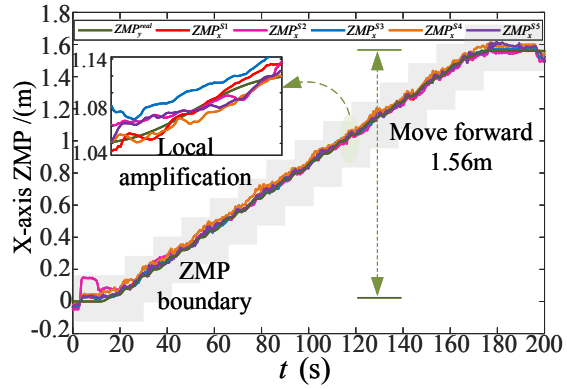

(a) The ZMP in the sagittal plane of all subjects

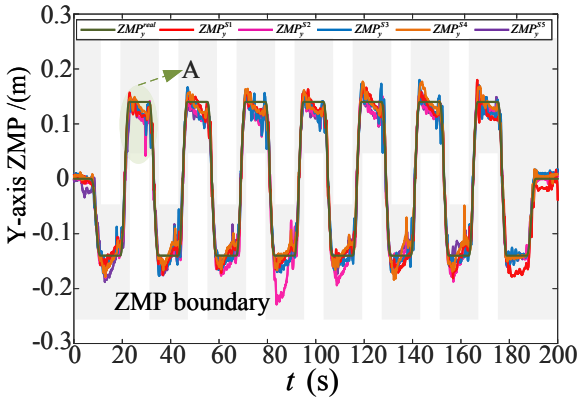

(b) The ZMP in the frontal plane of all subjects

Fig. 6. The responses of ZMP in walking of five subjects wearing the exoskeleton. Specifically, this includes the responses of ZMP in the sagittal (X axis) and frontal plane (Y axis).

Before the walking experiment, we set up the parameters of the DRN-FOV controller. The control parameters were set to z^{w}_{CoM}= 0.93(m), E= $\begin{bmatrix} 4000 & 2000 & 0 \end{bmatrix}$, η= $\begin{bmatrix} 2000 & 3000 & 0 \end{bmatrix}$, α= 0.4 for the sagittal plane (X axis) and α= 0.1 for the frontal plane (Y axis). These control parameters are chosen based on the inspired by the theory of humanoid robotics [35], and can be used in practical applications with only a little adjustment to obtain better experimental results. The controller parameters set do not need to be readjusted when applied across different subjects. Thus, the advantage of the proposed control method is that it does not depend on the body parameters of subjects, making it a simple application method.

C. Walking experiments on five sujects

The control objective of stable walking with the LLEs is shown in Eq. 2, that is, the response of ZMP during walking should always remains within the supporting polygon of both feet. Experimental snapshots of five subjects walking seven gait cycles are shown in Fig. 5. The complete walking experiment video can be found in [34]. The subjects completed stable walking on a flat road under the supervision of the investigator. Fig. 6 shows the response of ZMP of all subjects during walking with the LLEs. As shown in Fig. 6 (a), the actual ZMP in the X direction of all subjects always stays within the supporting polygon (gray area). It can be observed from the local amplification that the actual ZMP curve converges to the reference ZMP curve. Similarly, as shown in Fig. 6 (b), the actual ZMP in the Y direction of all subjects also remains within the gray area. When the leg of the LLEs transitions from the swing phase to the support phase, the impact force between the foot and the ground increases at the initial landing, causing a larger deviation of ZMP (e.g., point A in Fig. 6 (b)), but it quickly converges to near the desired

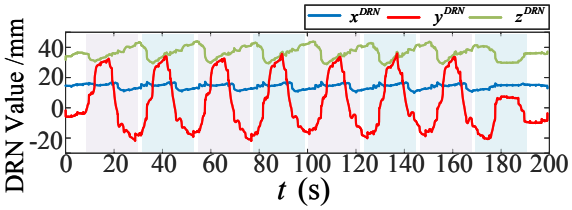

(a) The estimates position of S1

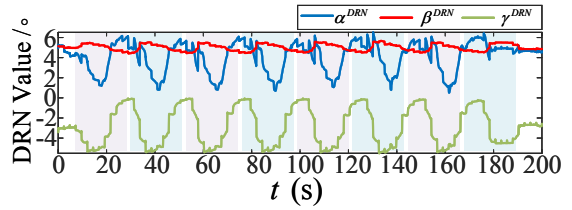

(b) The estimates rotation of S1

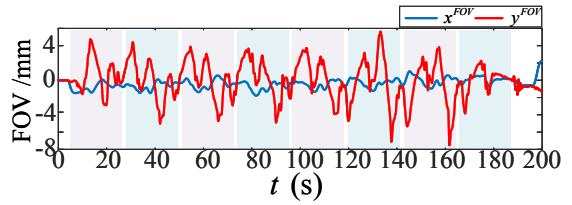

(c) The compliance control value of S1

Fig. 7. The control values of the proposed method, including deformations estimates for 3D position and rotation, viscoelastic control values.

ZMP position. Both in the X axis and Y axis directions, the peak ZMP is detected in a very short time and then converges quickly. In other words, the proposed DRN-FOV method exhibits viscoelasticity, absorbing external impacts, thus achieving stable walking.

We provide the control values in experiments to show the ability of the proposed controller to compensate for deformations. As shown in Fig. 7, due to space constraints, we only display the actual control values of S1, while the information for the remaining subjects can be found in [34]. All control values of S1 exhibit a periodic pattern, indicating the variation of the control values is related to the gait period. The maximum value of the 3D position estimation of the CoM is 44.092(mm), the maximum value of the 3D rotation estimation of the CoM is 6.555(°), and the maximum value of the compliance control is not more than 10(mm). Therefore, the compensation value of the DRN is larger than the compensation of the FOV. This confirms that the main function of the DRN is to compensate for the deformations of the LLEs in 3D position and 3D rotation, while the FOV primarily provides compliance to the LLEs, enabling it to walk smoothly.

During the walking process, the statistical results of ZMP errors and control values of all subjects are shown in Table II. The results are reported in the form of mean and standard error (SE). From Table II, it can be seen that the proposed controller compensates the most in the exoskeleton position with $z^{DRN} = 37.64 \pm 1.09$(mm), helping the actual CoM of the exoskeleton to move to the desired position. In the X and Y directions, the errors of the ZMP are 0.0213 $\pm$ 0.01(m) and 0.0138 $\pm$ 0.001(m), respectively. This indicates that the actual ZMP of the exoskeleton converges to the desired ZMP, which is also confirmed in Fig. 6.

V. Discussion and Conclusions

A. Discussion

The advantages of the proposed DRN-FOV control method can be summarized as follows:

(1) Unlike building complex state estimation models [10], [14], [19], we have developed a simple and direct estimation network. At each control cycle, using raw plantar force data as input, it can online estimate the variables of deformations of the LLEs. The experimental results are shown in Fig. 5 and Fig. 7. Therefore, we can conclude that the proposed controller can accurately estimate the deformations of the LLEs using only data from the 6-axis F/T sensor as control input.

(2) The exoskeleton walking without the DRN-FOV controller, as shown in Fig. 1 (right), there is an irreversible deformations that causes the exoskeleton to lose balance. However, with the DRN-FOV controller, we successfully completed a stable hands-free flat walking experiment for five subjects with different body parameters. The results of the walking experiments in Fig. 6 show that the viscoelasticity of DRN-FOV method eliminates external shocks and deformations, ensuring that the response of ZMP of different subjects remains within the supporting polygon. In practical applications, it is important to note that the designed controller does not require setting controller hyperparameters according to the individual body parameters of each subject. This distinguishes it from whole-body dynamic-based controllers [17], [18]. Therefore, we can conclude that the proposed controller can accurately estimate the deformations variables of the LLEs with different subjects, thus achieving stable walking.

B. Conclusions

This paper proposes a simple and direct closed-loop controller that can estimate the overall deformations of the LLEs using only data from the 6-axis F/T sensors. We have constructed an end-to-end deformations relationship estimation network and introduced a fractional viscoelasticity controller to achieve compliant stabilized walking for the LLEs. The effectiveness of the proposed controller was verified through walking experiments with five subjects. The results demonstrated that the method can accurately estimate the overall deformations of the LLEs and enables stable hands-free walking on flat terrain. Future work will explore how to extend this method to the LLEs walking on uneven terrains.

References

[1] C. Siviy, L. M. Baker, B. T. Quinlivan, F. Porciuncula, K. Swaminathan, L. N. Awad, and C. J. Walsh, "Opportunities and challenges in the development of exoskeletons for locomotor assistance," *Nature Biomedical Engineering*, vol. 7, no. 4, pp. 456–472, 2023.

[2] A. M. Dollar and H. Herr, "Lower extremity exoskeletons and active orthoses: challenges and state-of-the-art," *IEEE Transactions on robotics*, vol. 24, no. 1, pp. 144–158, 2008.

[3] M. Brunet, M. Pétriaux, F. Di Meglio, and N. Petit, "Enabling safe walking rehabilitation on the exoskeleton atalante: experimental results," *arXiv preprint arXiv:2304.08091*, 2023.

[4] T. Gurriet, M. Tucker, A. Duburcq, G. Boeris, and A. D. Ames, "Towards variable assistance for lower body exoskeletons," *IEEE Robotics and Automation Letters*, vol. 5, no. 1, pp. 266–273, 2019.

[5] E. R. Westervelt, J. W. Grizzle, C. Chevallereau, J. H. Choi, and B. Morris, *Feedback control of dynamic bipedal robot locomotion*. CRC press, 2018.

[6] D. Pinto-Fernandez, D. Torricelli, M. del Carmen Sanchez-Villamanan, F. Aller, K. Mombaur, R. Conti, N. Vitiello, J. C. Moreno, and J. L. Pons, "Performance evaluation of lower limb exoskeletons: a systematic review," *IEEE Transactions on Neural Systems and Rehabilitation Engineering*, vol. 28, no. 7, pp. 1573–1583, 2020.

[7] A. Martinez, B. Lawson, and M. Goldfarb, "A controller for guiding leg movement during overground walking with a lower limb exoskeleton," *IEEE Transactions on Robotics*, vol. 34, no. 1, pp. 183–193, 2017.

[8] A. Martinez, B. Lawson, C. Durrough, and M. Goldfarb, "A velocity-field-based controller for assisting leg movement during walking with a bilateral hip and knee lower limb exoskeleton," *IEEE Transactions on Robotics*, vol. 35, no. 2, pp. 307–316, 2018.

[9] T. Gurriet, M. Tucker, C. Kann, G. Boeris, and A. D. Ames, "Stabilization of exoskeletons through active ankle compensation," *arXiv preprint arXiv:1909.11848*, 2019.

[10] M. Vigne, A. El Khoury, F. Di Meglio, and N. Petit, "State estimation for a legged robot with multiple flexibilities using imus: A kinematic approach," *IEEE Robotics and Automation Letters*, vol. 5, no. 1, pp. 195–202, 2019.

[11] O. Harib, A. Hereid, A. Agrawal, T. Gurriet, S. Finet, G. Boeris, A. Duburcq, M. E. Mungai, M. Masselin, A. D. Ames *et al.*, "Feedback control of an exoskeleton for paraplegics: Toward robustly stable, hands-free dynamic walking," *IEEE Control Systems Magazine*, vol. 38, no. 6, pp. 61–87, 2018.

[12] A. Duburcq, F. Schramm, G. Boéris, N. Bredeche, and Y. Chevaleyre, "Reactive stepping for humanoid robots using reinforcement learning: Application to standing push recovery on the exoskeleton atalante," in *2022 IEEE/RSJ International Conference on Intelligent Robots and Systems (IROS)*. IEEE, 2022, pp. 9302–9309.

[13] E. Barıs, Y. Wen, S. J. Kim, M. R. Short, D. Ludvig, L. Hargrove, E. J. Perreault, K. M. Lynch, J. L. Pons *et al.*, "Haptic transparency and interaction force control for a lower-limb exoskeleton," *IEEE Transactions on Robotics*, 2024.

[14] M. Vigne, A. El Khoury, M. Pétriaux, F. Di Meglio, and N. Petit, "Movie: A velocity-aided imu attitude estimator for observing and controlling multiple deformations on legged robots," *IEEE Robotics and Automation Letters*, vol. 7, no. 2, pp. 3969–3976, 2022.

[15] J. W. Grizzle, C. Chevallereau, R. W. Sinnet, and A. D. Ames, "Models, feedback control, and open problems of 3d bipedal robotic walking," *Automatica*, vol. 50, no. 8, pp. 1955–1988, 2014.

[16] M. Brunet, M. Pétriaux, F. Di Meglio, and N. Petit, "Fast replanning of a lower-limb exoskeleton trajectories for rehabilitation," *2022 IEEE 61st Conference on Decision and Control (CDC)*, pp. 2039–2046, 2022.

[17] A. Agrawal, O. Harib, A. Hereid, S. Finet, M. Masselin, L. Praly, A. D. Ames, K. Sreenath, and J. W. Grizzle, "First steps towards translating hzd control of bipedal robots to decentralized control of exoskeletons," *IEEE Access*, vol. 5, pp. 9919–9934, 2017.

[18] T. Gurriet, S. Finet, G. Boeris, A. Duburcq, A. Hereid, O. Harib, M. Masselin, J. Grizzle, and A. D. Ames, "Towards restoring locomotion for paraplegics: Realizing dynamically stable walking on exoskeletons," *2018 IEEE international conference on robotics and automation (ICRA)*, pp. 2804–2811, 2018.

[19] F. E. Xavier, G. Burger, M. Pétriaux, J.-E. Deschaud, and F. Goulette, "Multi-imu proprioceptive state estimator for humanoid robots," *2023 IEEE/RSJ International Conference on Intelligent Robots and Systems (IROS)*, pp. 10 880–10 887, 2023.

[20] G. Loianno, C. Brunner, G. McGrath, and V. Kumar, "Estimation, control, and planning for aggressive flight with a small quadrotor with a single camera and imu," *IEEE Robotics and Automation Letters*, vol. 2, no. 2, pp. 404–411, 2016.

[21] M. K. Al-Sharman, Y. Zweiri, M. A. K. Jaradat, R. Al-Husari, D. Gan, and L. D. Seneviratne, "Deep-learning-based neural network training for state estimation enhancement: Application to attitude estimation," *IEEE Transactions on Instrumentation and Measurement*, vol. 69, no. 1, pp. 24–34, 2019.

[22] A. Vaswani, N. Shazeer, N. Parmar, J. Uszkoreit, L. Jones, A. N. Gomez, Ł. Kaiser, and I. Polosukhin, "Attention is all you need," *Advances in neural information processing systems*, vol. 30, 2017.

[23] H. Zhou, S. Zhang, J. Peng, S. Zhang, J. Li, H. Xiong, and W. Zhang, "Informer: Beyond efficient transformer for long sequence time-series forecasting," *Proceedings of the AAAI conference on artificial intelligence*, vol. 35, no. 12, pp. 11 106–11 115, 2021.

[24] M. Zhao, J. Peng, S. Yu, L. Liu, and N. Wu, "Exploring structural sparsity in cnn via selective penalty," *IEEE Transactions on Circuits and Systems for Video Technology*, vol. 32, no. 3, pp. 1658–1666, 2021.

[25] S. Lin, R. Ji, Y. Li, C. Deng, and X. Li, "Toward compact convnets via structure-sparsity regularized filter pruning," *IEEE transactions on neural networks and learning systems*, vol. 31, no. 2, pp. 574–588, 2019.

[26] P. Shah and S. Agashe, "Review of fractional pid controller," *Mechatronics*, vol. 38, pp. 29–41, 2016.

[27] K. Bingi, B. Rajanarayan Prusty, and A. Pal Singh, "A review on fractional-order modelling and control of robotic manipulators," *Fractal and Fractional*, vol. 7, no. 1, p. 77, 2023.

[28] A. Dumlu and K. Erenturk, "Trajectory tracking control for a 3-dof parallel manipulator using fractional-order $\mathrm{pI}^{\lambda}\mathrm{D}^{\mu}$ control," *IEEE Transactions on Industrial Electronics*, vol. 61, no. 7, pp. 3417–3426, 2013.

[29] W. Jie, Z. Yudong, Y. Bao, H. H. Kim, and M. C. Lee, "Trajectory tracking control using fractional-order terminal sliding mode control with sliding perturbation observer for a 7-dof robot manipulator," *IEEE/ASME Transactions on Mechatronics*, vol. PP, no. 99, pp. 1–1, 2020.

[30] P.-B. Wieber, R. Tedrake, and S. Kuindersma, "Modeling and control of legged robots," *Springer handbook of robotics*, pp. 1203–1234, 2016.

[31] T. Karner, J. Gotlih, B. Razboršek, T. Vuherer, L. Berus, and K. Gotlih, "Use of single and double fractional kelvin–voigt model on viscoelastic elastomer," *Smart Materials and Structures*, vol. 29, no. 1, p. 015006, 2019.

[32] D. Tian, F. Li, M. Yang, Z. Chen, J. Li, Z. Yi, L. Zhang, and X. Wu, "Deformation estimator network-based feedback control for wearable exoskeleton with body disturbances: Toward stable and dynamic walking," *IEEE Transactions on Systems, Man, and Cybernetics: Systems*, vol. 54, no. 9, pp. 5844–5856, 2024.

[33] J. Liu, Y. He, J. Yang, W. Cao, and X. Wu, "Design and analysis of a novel 12-dof self-balancing lower extremity exoskeleton for walking assistance," *Mechanism and Machine Theory*, vol. 167, p. 104519, 2022.

[34] "A closed-loop control for lower limb exoskeletons considering overall deformation: A simple and direct application method," [Online]. Available: https://youtu.be/BhHPOBsZqHs.

[35] Q. Li, Z. Yu, X. Chen, L. Meng, and C. Tao, "A compliance control method based on viscoelastic model for position-controlled humanoid robots," *IEEE/RSJ International Conference on Intelligent Robots and Systems (IROS)*, 2020.